

Article

The Effect of Arm Movements on the Dynamics of the Wheelchair Frame during Manual Wheelchair Actuation and Propulsion

Franz Konstantin Fuss^{1,2,*}, Adin Ming Tan^{2,3} and Yehuda Weizman^{2,4} 

- ¹ Division of Biomechanics, Fraunhofer Institute for Manufacturing Engineering and Automation IPA, D-95447 Bayreuth, Germany
- ² Chair of Biomechanics, Faculty of Engineering Science, University of Bayreuth, D-95440 Bayreuth, Germany; amtan@swin.edu.au (A.M.T.); yehuda.weizman@uni-bayreuth.de (Y.W.)
- ³ Faculty of Health, Arts and Design, Swinburne University, Melbourne, VIC 3000, Australia
- ⁴ Department of Health and Medical Science, School of Health Science, Swinburne University of Technology, Hawthorn, VIC 3122, Australia
- * Correspondence: franz.konstantin.fuss@ipa.fraunhofer.de or franzkonstantin.fuss@uni-bayreuth.de

Abstract: Wheelchair propulsion and actuation are influenced by the moving masses of the wheelchair user; however, the extent of this effect is still unclear. The main evidence of this effect is that the speed of the wheelchair frame continues to increase after the end of the push phase. The wheelchair's speed was measured using IMUs and the duration of the push period was recorded using miniaturised pressure sensors attached to the driver's middle fingers. The velocity and acceleration were determined for various average stroke cycle speeds to determine the speed dependency of the acceleration. The wheelchair was then mounted on a force plate to measure the inertial forces of the hands moving back and forth. The aerodynamic drag and rolling resistance forces were determined from coast-down experiments. Based on the measured forces, the behaviour of the force and velocity profiles was finally modelled by gradually reducing the mass of the arms and thus their inertial force. The results showed that the wheelchair is accelerated throughout the push phase (except for a temporary deceleration in the middle of the push phase at higher velocities), and that this acceleration continues well after the push phase. In the second half of the recovery phase, the wheelchair decelerates. The horizontal inertial forces measured on the force plate are predominantly negative in the push phase and in the second half of the recovery phase, and positive in the first half of the push phase, and their impulse is zero due to the conservation of momentum. Modelling the wheelchair with moving masses showed that reducing the horizontal inertial forces has no effect on the driver's propulsive force but reduces the velocity fluctuations. The main conclusion of this research is that the wheelchair user's power should be calculated only from the pure propulsive force that is required in the push phase to overcome the dissipative forces and that enables the gain or loss in speed per stroke cycle, but not directly from the measured velocity.

Keywords: wheelchair actuation; inertial forces; dissipative forces; propulsive force; wheelchair model; conservation of momentum; velocity; acceleration; moving masses; power



Citation: Fuss, F.K.; Tan, A.M.; Weizman, Y. The Effect of Arm Movements on the Dynamics of the Wheelchair Frame during Manual Wheelchair Actuation and Propulsion. *Actuators* **2024**, *13*, 183. <https://doi.org/10.3390/act13050183>

Academic Editor: Alessio Merola

Received: 29 March 2024

Revised: 8 May 2024

Accepted: 10 May 2024

Published: 11 May 2024



Copyright: © 2024 by the authors. Licensee MDPI, Basel, Switzerland. This article is an open access article distributed under the terms and conditions of the Creative Commons Attribution (CC BY) license (<https://creativecommons.org/licenses/by/4.0/>).

1. Introduction

A system consisting of a user and a wheelchair is evidently not a rigid body moving in the global coordinate system (GCS). If the frame of the wheelchair moves forward on a straight path (translational velocity $v_x > 0$, angular velocity $\omega_{xyz} = 0$), then the wheels rotate about their axle relative to the frame and about their centre of pressure in the GCS (rolling motion). The user's trunk (if the user is capable of trunk movements) and the segments of the upper limbs oscillate. These moving masses account for the fact that the centre of mass (COM) of the entire system is constantly moving relative to the wheelchair frame rather

than occupying a constant position like a rigid body. In this context, Vanlandewijck et al. [1] distinguished three phases of the stroke cycle: the push phase, characterised by a positive propulsive force throughout the entire phase; the early recovery phase, with an equally positive propulsive force; and the late recovery phase, with a negative propulsive force. Vanlandewijck et al. [1] attributed this phenomenon to the significant increase in mechanical work during the recovery phase, caused by trunk and arm movements that induce inertial forces to act on the wheelchair. Similarly, van Dijk et al. [2] found that 25–30% of the total forward propulsive impulse per push due to trunk motion was performed in the recovery phase after hand release. Poulet et al. [3] reported that “*a second peak in velocity is usually assumed to be caused by the inertia of the trunk*”. Furthermore, Poulet et al. [3] assumed that “*the presence of a second velocity peak . . . can either be associated to the inertia of the athletes’ arms or to their propulsion technique*” in wheelchair racers specifically classified as T2, incapable of trunk movements. Kawabata et al. [4] suggested that “*trunk extension caused by reaction forces generated by pushing of the hand-rim contributes to increased wheelchair velocity during the recovery phase*”. Moss et al. [5] also report in wheelchair racers that the peak velocity occurs after release and attribute this effect to the backward movement of the head and trunk, which increases the velocity of the wheelchair and the forward movement of the head and trunk, causing a retarding effect on the wheelchair. Masson et al. [6] modelled the limb momentum to power transfer and concluded that both the upper limb momentum and muscles contribute to wheelchair pushing.

A simple experiment demonstrates and explains the effect of mass movements in the user–wheelchair system: sitting upright in the chair without moving the trunk and solely moving the fists rapidly back and forth leads to a noticeable and measurable forward–backward movement of the wheelchair frame, simply due to the conservation of linear momentum.

Since the translational velocity of the moving system’s COM (v_{COM}) cannot be measured outside a biomechanics laboratory, the speed of the entire system is usually expressed as the speed of the wheelchair frame v_{Fx} . This speed is easily measured using IMUs, particularly from the angular velocity data of the gyros, and then converted into the translational velocity of the frame if the radius r of the wheel and its camber angle θ are known [7].

The stroke cycle of wheelchair propulsion is divided into two phases: the push phase and the recovery phase. The former is defined by the contact between the user’s hand and the pushrim, or, more precisely, the period during which the user’s hand imparts a torque on the wheel. Mere contact does not produce the normal force required to create the friction force on the pushrim, which in turn imparts torque to the wheel. The detection of the exact start (‘hand strike’) and end (‘hand-off’) of the push phase is crucial but has disadvantages. There are several methods to choose from, which are briefly explained below.

- (1) Force and torque data obtained from force transducers or strain gauges:

The following commercially available systems measure wheel speed and the forces and torques exerted by the user at the pushrim:

- (a) The Mayo Clinic’s instrumented wheel (6-DOF load cell) developed by Wu [8];
- (b) The SMARTWheel (strain gauged), developed by Cooper [9], available from Three Rivers Holdings (Mesa, AZ, USA);
- (c) The OptiPush Biofeedback System (6-DOF load cell) developed by Richter [10].

Other systems are based on force transducers, e.g., one 3-DOF [11] or four 2-DOF [12] transducers.

The contact of the hand with the pushrim is detected by the sensors, regardless of whether it involves braking or propulsive forces. Any force or torque greater than zero is suitable for defining the push force. If there is background noise, a threshold can be applied. Guo et al. [10] and de Vries et al. [13], for example, used thresholds of 1 and 2 Nm, respectively.

These technical solutions are very precise but cannot be applied to standard wheelchair wheels.

(2) Angular velocity data obtained from an IMU:

Quoting de Vries et al. [13]: *“For push detection from IMU data, the following basic assumption was made: in all-day wheelchair propulsion, when propulsive force is exerted at the rim, the angular velocity will increase. When there is no longer a force exerted, the angular velocity will decrease due to resistive forces”*. Accordingly, a peak detection algorithm was used to identify the start and end of the push phase. From *figure 4b* in the publication by de Vries et al. [13], the maximum average velocity was about $300^\circ/\text{s}$ (5.236 rad/s). As de Vries et al. [13] used a 24-inch SMARTWheel, the wheel radius r was 0.305 m, resulting in a translational velocity v_x of 1.6 m/s (5.75 kph). As shown later in Section 3, the velocity peak (which according to de Vries et al. [13] indicates the end of the push phase) occurs 23% (of the stroke cycle) **after** the end of the push phase (at an average cycle speed of 1.6 m/s). It is therefore not surprising that de Vries et al. [13] reported: *“... the push durations derived from the IMU data were longer than those from the Smartwheel data ...”*.

(3) Translational acceleration data obtained from an IMU:

Lewis et al. [14] connected IMUs to *“the left and right axle housings of the wheelchair frame”* to measure the translational acceleration. The *“contact and release points [between the hands and the pushrim] were automatically detected using a custom peak-detection algorithm”* [14]. Lewis et al. [14] reported that *“IMUs were effectively capable of automatically identifying contact, however the algorithm located release less reliably, without also detecting noise ...”*. Lewis et al. [14] concluded that *“At this stage automatic detection of release points is not plausible”*.

(4) Motion analysis systems:

Apparently, Lewis et al. [14] used two different methods concurrently:

- (a) High-speed Sony PXW-FS7 video cameras, the data of which *“was manually digitised ... with hand contact and release identified as the first and last frame where any part of the athlete’s hand or glove was in contact with the pushrim, respectively”*.
- (b) A VICON system was used for measuring the translational acceleration. The extreme (peak/trough) data of positive and negative acceleration waves were considered as the end and the beginning of the push phase, respectively. However, the location of the marker whose acceleration was measured is unclear. There is a transition from negative to positive acceleration during the alleged push phase (cf. *figure 2* in the publication of Lewis et al. [14]). If the marker were placed on the user’s hand, then the user would have decelerated in the first part of the push phase and accelerated in the second part.

Lewis et al. [14] did not cross-validate the two motion analysis methods they used. The problem with motion analysis systems is that the space where the cameras can be used for data capture is limited and, therefore, they are not suitable for continuous data recording.

(5) Pushrim-based push-phase detection systems:

Basteris et al. [15] developed a capacitive touch sensor by placing a thin conductive wire over the pushrim to detect the contact between the skin and the pushrim. They connected the touch sensor output to two infrared LEDs that were detected by an Elite motion analysis system for synchronisation purposes.

Van Dijk et al. [2] developed a *“Rim Hit Detection”* system by using *“two strips of conductive (woven nickel-copper alloy) tape, placed closely parallel to each other along the perimeter of the pushrim. A voltage of 3.5 V was applied to one of the strips to measure short circuit of the system due to hand contact”*.

Pushrim-based recording systems must be specifically installed on the pushrim. They would not work when wearing gloves. In the *“Rim Hit Detection”* system developed by van Dijk et al. [2], metal tapes or conductive fabric would have to be attached to the gloves to achieve a short circuit. Metal tapes attached to the pushrim are a potential source of hand injury if gloves are not worn.

Based on the fluctuating speed during the push phase, Basteris et al. [15] calculated time- and speed-based efficacy indices and assumed that the decelerations are associated with inefficient coupling of the hand and the pushrim. The fluctuating speed profile is shown in *figure 3* in the publication by Basteris et al. [15], which also displays an increasing speed immediately after releasing the pushrim. This phenomenon matches the findings of Vanlandewijck et al. [1] and van Dijk et al. [2], but Basteris et al. [15] did not further explain this paradox.

The aim of this study was to investigate the phenomenon of moving masses within the user–wheelchair system by analysing velocity and acceleration profiles and measuring the dynamic effect of these moving masses by modelling the force profiles acting on the user–wheelchair system with and without moving masses.

2. Methods

2.1. Objective of the Method

The methodological approach consisted of a sequence of individual methods, experiments and a wheelchair model to shed light on the effect of moving masses when driving a wheelchair. These moving masses include, for example, the trunk and the arms of the wheelchair user.

The first experiment (Figure 1) served to record and analyse speed profiles when driving a wheelchair at different speeds, instrumented with IMUs, and to verify the phenomenon of speed increase after ‘hand-off’, i.e., at the beginning of the recovery phase. For this purpose, the exact times of hand-strike and hand-off had to be determined. The speed profiles were used to extract the accelerations of the wheelchair frame and their velocity-dependency. Since these horizontal accelerations produce ‘virtual’ inertial forces according to d’Alembert’s principle [16], corresponding to the (negative) product of mass and acceleration, there must be other forces that are in equilibrium with these inertial forces, which are not necessarily just the propulsive force (during the push phase) and the dissipative forces (drag and rolling resistance throughout the stroke cycle).

Therefore, in the second experiment, a wheelchair was mounted on a force plate so that its large rear wheels were not in contact with the ground to measure the horizontal and vertical forces exerted on the static wheelchair while the arms and wheels were moved in the same way as in a wheelchair rolling on firm ground.

The data obtained from the first and second experiments served to model the influence of moving masses on the velocity profile of a wheelchair when driven by the user. To do this, the momentum of the moving masses was gradually reduced by changing their amount of mass but maintaining their speed.

2.2. Experiment 1

For all experiments, a manual Otto Bock Ventus wheelchair (Figure 1a) was used. The chair had 24-inch wheels (diameter 0.61 m, $r = 0.305$ m) with a camber angle θ of 3.2° and a track width of 0.56 m. The chair was equipped with IMUs (3-Space™ Wireless 2.4 GHz DSSS, Yost Labs, Portsmouth, OH, USA; Figure 1a,b) attached to the wheel hubs. The gyro data recorded by the IMUs at 100 Hz were transmitted wirelessly to a receiver (3-Space™ Wireless Dongle, Yost Labs, Portsmouth, OH, USA; Figure 1b), which was connected to a laptop via a USB cable. In this experiment, the velocities and accelerations calculated from the gyro data refer to the speed and acceleration of the wheelchair frame. The experiments were carried out indoors in a 30 m-long former factory hall with a rubber mat floor, adjacent to the Medical Technology and Sports Engineering laboratory at Swinburne University. The wheelchair was driven by an able-bodied researcher (F.K.F) with 15 years of extensive research experience in handling and driving wheelchairs. This experience was essential to safely achieve top speeds of up to 2.78 m/s (10 kph) in the 30 m-long hall to accelerate the wheelchair to the desired travel speed. This speed was maintained consistently for at least a few strokes, and finally the wheelchair was slowed down safely but quickly before it reached the end of the hall (Figure 2). The participant did not move

his trunk during all experiments because he felt that the trunk movement prevented him from reaching high speeds in the sense that his oscillating trunk cannot keep up with the speed of his reciprocating hands. To detect the contact between hands and pushrims, the wheelchair driver was equipped with a wearable pressure sensor system (Figure 1c,d). After experimenting with pushrim-based touch sensing, the new type of instrumentation was easier and faster to deploy. For this purpose, a small piezoresistive pressure sensor was taped to the palmar side of the mid-segment of each middle finger (Figure 1c), as the participant had to firmly grip the pushrim to apply the required normal force to generate the propulsive force. The pressure sensors on both sides were connected to a programmable microcontroller (TEENSY 3.2, 32-bit ARM, Cortex-M4 72 MHz CPU, Portland, OR, USA; Figure 1d), a 3.7 V battery and a data logger (OpenLog, SparkFun Electronics, Boulder, CO, USA). This setup enabled the recording of voltage fluctuations, caused by the changing resistance of the sensors, across a reference resistor with a frequency of 200 Hz (twice the frequency of that of the IMU was required for synchronisation purposes). Ethics approval was granted by the Human Ethics Committee of Swinburne University (approval no. 2019/106) in adherence with the Declaration of Helsinki.

The raw gyro data recorded by the two IMUs at 100 Hz were processed using the method of Fuss [7], which calculates the true wheel speed, frame speed, frame acceleration, distance travelled, turning angular velocity, turning radius, power and energy expenditure. In addition to the gyro data, the acceleration data of the IMUs were recorded to synchronise the data of the IMUs with the pressure sensor data recorded at 200 Hz (twice the frequency of that of the IMU was required for synchronisation purposes). To achieve this, the wheelchair user hit the pushrims with his fingers five times before and after each experiment. A total of ten impacts were recorded by both the pressure sensors and the accelerometers. The pressure sensor data (sensor conductance in Siemens) and the accelerometer data (in g , recorded at 100 Hz) were then matched using a data fusion algorithm based on the 10 impacts. The unloaded pressure sensors had a resistance of approximately 100 k Ω (conductance of 0.01 mS), and less than 20 Ω (conductance of 50 mS) when loaded and driving the wheelchair at 2.6 m/s. The push phase was defined by the conductance signal exceeding a threshold of 0.1 mS (Figure 3).

For the data analysis, speed segments with a nearly constant translational velocity defined by an acceleration within $\pm 0.1 \text{ m/s}^2$, calculated from the velocity averaged over 2.5 s, were selected. For each stroke cycle (right and left side), the following parameters were calculated: the average velocity; the stroke cycle period and frequency; and the push and recovery periods. The time axis of each stroke was normalised to the cycle time (one stroke cycle = unity or 100%). The normalised stroke time $t_{\%}$ was rounded to the nearest half percent so the normalised stroke time was divided into 201 bins. For each bin (or time slice), the average stroke velocity v_{avg} was correlated to the actual wheelchair frame velocity $v_{t\%}$, and the regression slope C_1 and intercept C_2 , and the coefficient of determination (R^2) were calculated. The instantaneous velocity $v_{t\%}$ was recalculated from C_1 and C_2 for any v_{avg} :

$$v_{t\%} = C_1 v_{\text{avg}} + C_2 \quad (1)$$

where i denotes the bin number. Additionally, the stroke cycle period (and push and recovery periods) was correlated to the average stroke velocity v_{avg} using a power law fitting function to convert $t_{\%}$ to t_i :

$$t_i = t_{\%} j_i v_{\text{avg}}^{b_i} \quad (2)$$

where j and b denote the multiplier and the exponent of the power function, respectively. The acceleration, a , associated with each bin was calculated from the following equation:

$$a_i = \frac{dv_i}{dt_i} \quad (3)$$

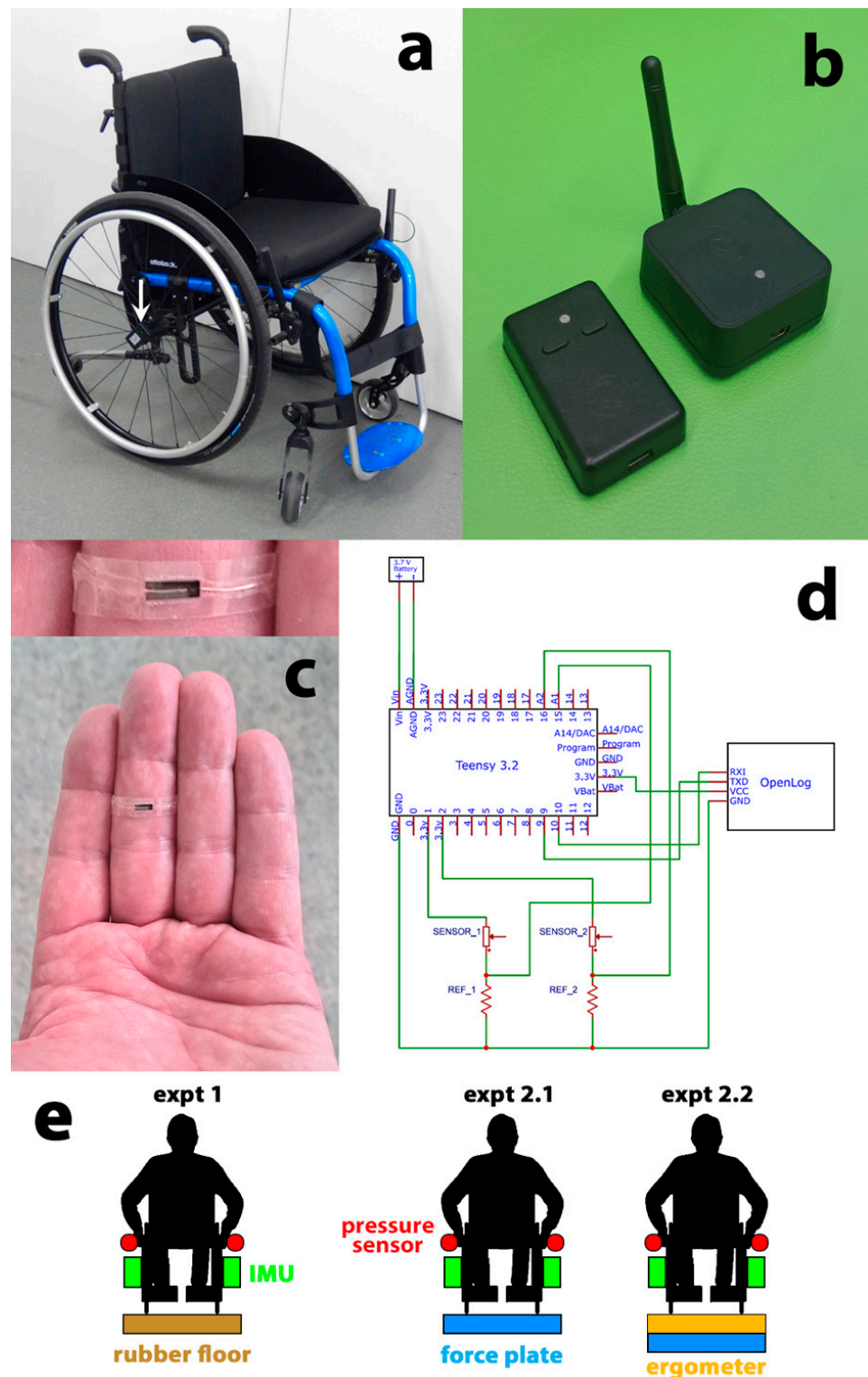


Figure 1. Wheelchair and measurement system; (a) Venustech wheelchair with sensor (white arrow) mounted on the wheel hub; (b) wireless IMU (left) and receiver with antenna (right); (c) miniaturised pressure sensor mounted on the middle finger; (d) circuit diagram of the pressure sensors; (e) equipment (colour coded) used in the different experiments (expt).

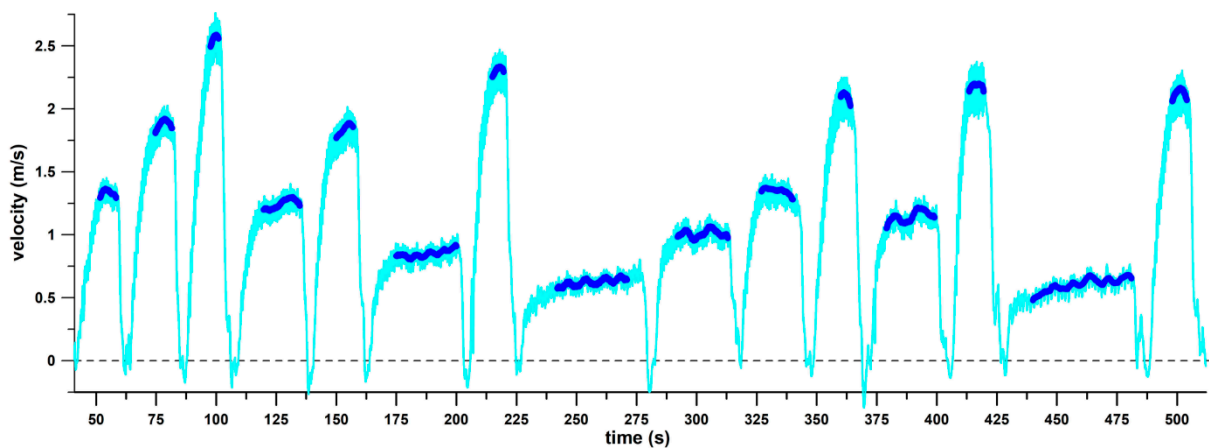


Figure 2. Velocity profile against time of a single experiment; the dark blue segments indicate a nearly constant translational velocity of a minimal acceleration within a $\pm 0.1 \text{ m/s}^2$ acceleration window; each of the 15 runs were carried out along the 30 m factory hall by changing the direction and turning after each run.

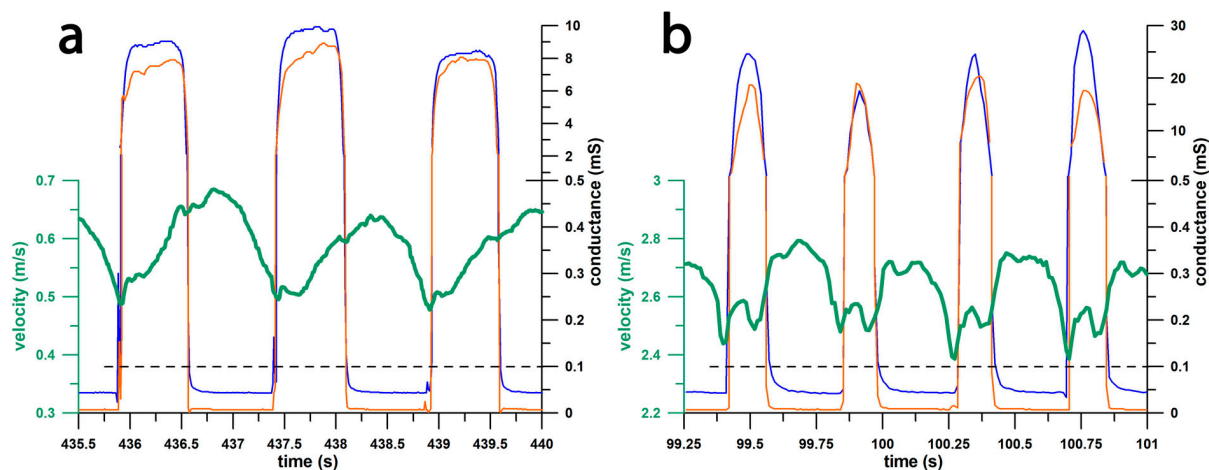


Figure 3. Slow (a) and fast (b) velocity profiles (green) against time; the push phase is identified from conductance data (blue and orange curves, right and left hand, respectively) larger than 0.1 mS (dashed line). Note that the resolution of the conductance scales changes at 0.5 mS .

2.3. Experiment 2

The wheelchair was mounted statically on a force plate (Kistler, Winterthur, Switzerland) by using the same IMUs and pressure sensors already described above. The only masses that moved in the horizontal and vertical directions relative to the force plate were the participant's arms. The reaction forces that balance the inertial forces of the arms were measured with the force plate at 200 Hz (twice the frequency of that of the IMU was required for synchronisation purposes). The force plate data, pressure sensor data and IMU data were synchronised using the method described above.

Initially, the wheels were unconstrained, and the participant drove them at different speeds. Since the velocity profiles differed from those in Experiment 1 due to insufficient deceleration of the wheels in the recovery phase, the wheels were constrained with an ergometer (Cycling Deal, Dandenong South, Australia) that was mounted on the force plate statically as the wheelchair was firmly placed on it. The rear wheels were in contact with the ergometer's rollers to provide the necessary resistance required to simulate the braking of the wheels during the recovery phase and to experience a more natural feeling in contrast to the freely spinning unconstrained wheels. The raw force data obtained from the

force plate served to understand and analyse the inertial forces generated by the moving arms. Furthermore, the impulse across the stroke cycle was calculated by integrating the horizontal (F_y) and vertical (F_z) forces over time. This refers to stroke cycles carried out at a relatively constant speed. Since the impulse S is equal to the change in linear momentum Δp , the impulse across a stroke cycle should ideally be zero if the wheels of a wheelchair are driven at a constant average angular velocity.

The equipment used in Experiments 1 and 2 is summarised in Figure 1e.

2.4. Wheelchair Model with Moving Masses

From first principles, particularly the law of the conservation of momentum, the momentum has the same magnitude both before and after an event. From a wheelchair dynamics perspective, this event is a signal stroke cycle. If the velocity of the wheelchair is the same at the beginning and at the end of the stroke cycle, and there is no loss or gain in mass, the momentum will be exactly the same at the start and end of the stroke cycle. This implies that the impulse is zero. This principle applies particularly to the propulsive force, which only acts in the push phase, and to the dissipative forces (rolling resistance, aerodynamic drag) throughout the entire stroke cycle. The integral of the sum of these forces over time must be zero, so the velocity at the beginning and at the end of the stroke cycle is the same.

The following forces acting in the horizontal direction were included in the model: the propulsive force PF , drag force DF , the friction force of the rolling resistance RF , the inertial force IF of the user–wheelchair system, and the inertial forces of the moving masses F_y .

From the force equilibrium:

$$PF + DF + RF + IF + F_y = 0 \quad (4)$$

From the basic condition for an average constant velocity, the propulsive and dissipative forces are in equilibrium:

$$\int (PF + DF + RF) dt = 0 \quad (5)$$

From the basic condition for an average constant velocity, the integral of the acceleration is zero:

$$\int IF dt = 0 \quad (6)$$

As a result of the force equilibrium:

$$\int F_y dt = 0 \quad (7)$$

The known variables in Equations (4)–(6) are IF , DF and RF . IF is calculated from the product of system mass and acceleration obtained from Equation (3). DF and RF were determined simultaneously from coast-down experiments [7,17,18]. Van Dijk et al. [19] claimed that “the information required to calculate air resistance cannot be derived from IMU data”. However, when solving the differential equation of a coasting wheelchair [17], we obtained the following solution:

$$v_t = \sqrt{\frac{c_2}{c_1}} \tan \left[\tan^{-1} \left(v_0 \sqrt{\frac{c_1}{c_2}} \right) - t \frac{\sqrt{c_1 c_2}}{m} \right] \quad (8)$$

where v_0 is the initial velocity at the beginning of the coasting process and constants $c_1 = 0.5 \rho A d + k m g$ and $c_2 = \mu m g$ (where ρ is the air density; $A d$ is the drag area, the product of drag coefficient and frontal area; m is the system mass; μ is the rolling friction coefficient; g is the gravitational acceleration). The constant k is the non-linear velocity-dependent term of the rolling friction, which is negligible at least in racing wheelchairs [17]. After processing the angular velocity obtained from the IMU’s gyroscopic sensors to

calculate the translational velocity of the coast-down experiment, fitting the latter with Equation (8) yields the coefficients c_1 and c_2 . DF is obtained by multiplying c_1 with v^2 , and $RF = c_2$. To calculate c_1 and c_2 , the participant performed five coasting experiments with his usual trunk position at different v_0 immediately before coast-down, and then continued rolling until the wheelchair came to a complete stop.

The unknown variables in Equations (4), (5) and (7) are PF and F_y . PF was calculated as a rectangular positive impulse in the push phase, which is in equilibrium with the negative DF and RF impulses throughout the stroke cycle. F_y results from the force equilibrium of Equation (4). For a continuous F_y function, the rectangular PF impulse had to be adjusted to a trapezoidal profile. After verifying that all forces satisfy the conditions of Equations (4)–(7), an average velocity of approximately 2.5 m/s was simulated by an initial velocity and an appropriate PF level, and the velocity profile of the stroke cycle was numerically calculated. To assess the effect of the inertia of the moving arm masses, the F_y force was incrementally reduced to zero and the velocity profile was recalculated. Reducing the F_y force corresponds to a virtual reduction in mass while maintaining the same speed of arm movement.

3. Results

3.1. Experiment 1

3.1.1. Experiment 1—Stroke Cycle

The data from 445 stroke cycles were examined. The average speed of the stroke cycles ranged from 0.586 (Figure 3a) to 2.626 m/s (Figure 3b); the minimum and maximum instantaneous speeds were between 0.504 to 2.761 m/s. At all speed levels, the velocity continued to increase after the end of the push phase (Figure 3). The distribution of the number of stroke cycles in relation to the average speed is shown in Figure 4.

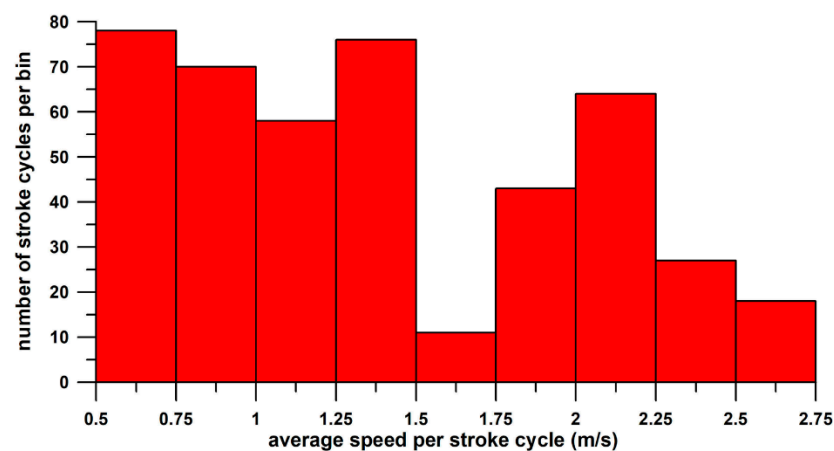


Figure 4. Distribution of the analysed stroke cycles across the range of the average speed per stroke cycle.

The duration of the stroke cycle correlated with the average speed of the stroke cycle (Figure 5a). The duration of the stroke cycle at minimum and maximum speeds was approximately 1.2 s and 0.4 s, respectively. Normalised to the stroke cycle, the end of the push phase (and the start of the recovery phase; Figure 5b) fluctuated more than the duration of the stroke cycle (Figure 5a) and decreased with an increasing average speed. At minimum and maximum speeds, the end of the push phase was found approximately at 37.7% and 34.4% of the stroke cycle (Figure 5b), respectively.

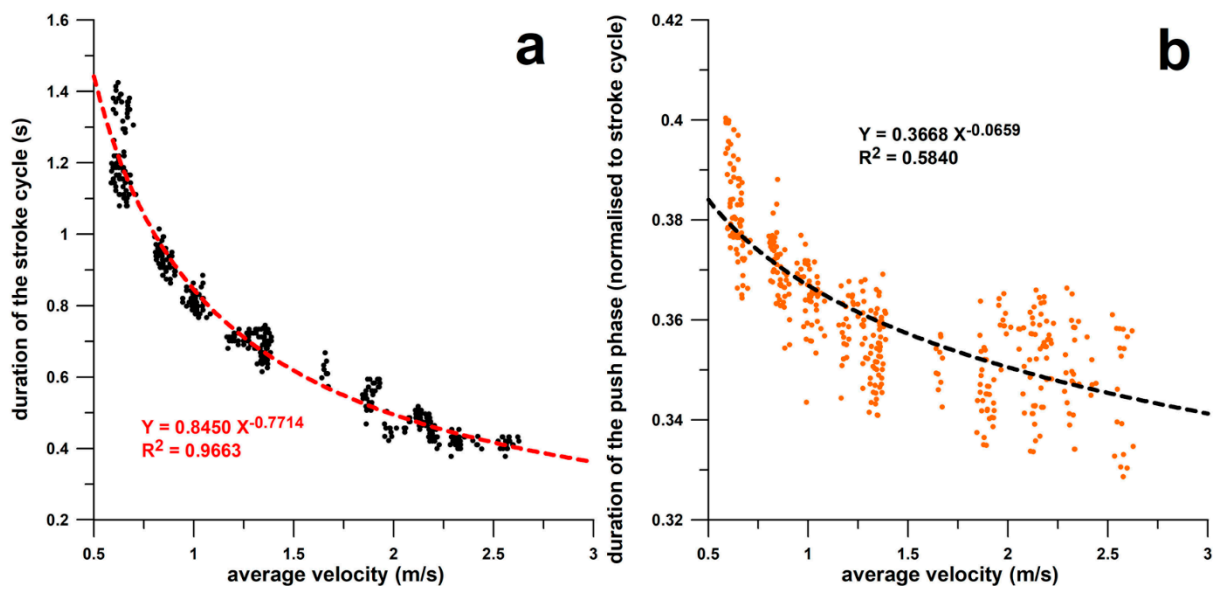


Figure 5. (a) Duration of stroke cycle against the average velocity; (b) duration of the push phase (normalised to the duration of the stroke cycle) against the average velocity. The data are fitted with a power function (dashed curves).

3.1.2. Experiment 1—Velocity Profiles

Figure 6a shows the correlation between instantaneous and average stroke velocity. Since the instantaneous velocity of each stroke cycle fluctuates around the average velocity, the slopes and gradients of the regression function are close to 1 and 0, respectively. The R^2 values of the individual regression functions across the stroke cycle were 0.9970 ± 0.0019 (0.9815–0.9995).

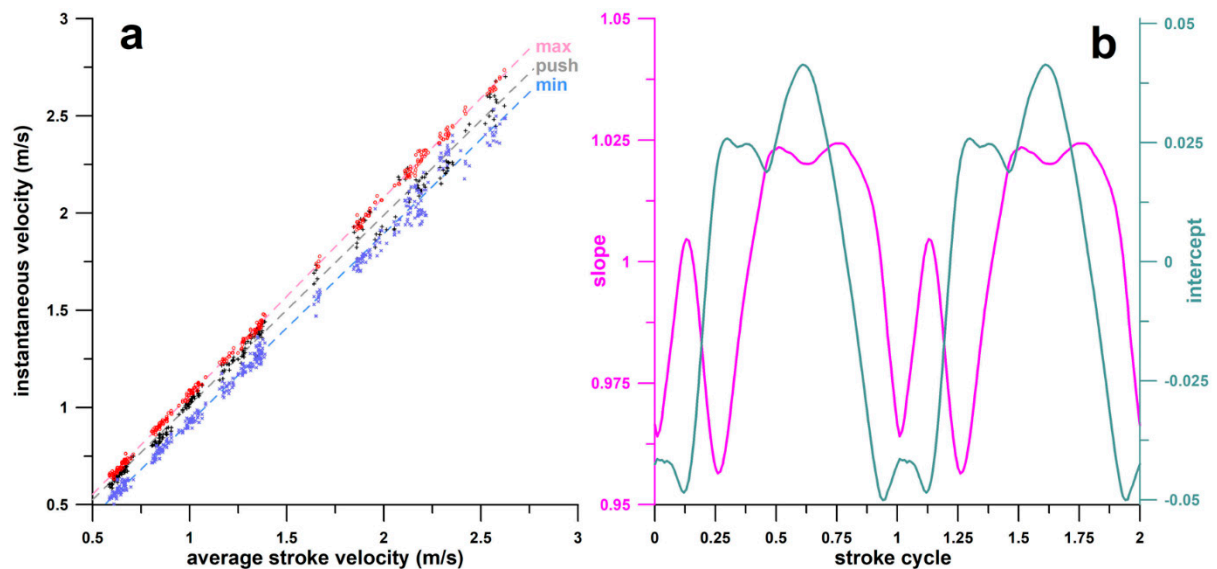


Figure 6. Method for calculating the average instantaneous velocity from the average stroke velocity: (a) Instantaneous velocity from the average stroke velocity; linear regression functions (dashed lines) at different stages of the stroke cycle: min = 0% of the stroke cycle (minimum velocity at the beginning of the push phase), push = 35.5% of the stroke cycle (end of push phase), and max = 60.5% of the stroke cycle (maximum velocity). (b) Slope and intercept of the linear regression functions against the stroke cycle.

From the slopes and gradients of the regression function (Figure 6b), the average velocity profiles associated with 11 average velocities were calculated (Figure 7a). At average velocities less than 1.25 m/s, the instantaneous velocity increases continuously from the beginning of the push phase to a maximum speed ('max' in Figure 7a) well after the end of the push phase, and then decreases continuously to the minimum speed at the end of the stroke cycle. At an average velocity of 1.25 m/s, a flat speed section (Figure 7a,b) at 20% of the stroke cycle interrupts the continuously increasing velocity profile. At an average velocity greater than 1.25 m/s, the speed of this flat segment decreases between 15% and 25% of the stroke cycle, producing a significant peak at 15% of the stroke cycle (upward arrow in Figure 7b). Figure 8 shows the data of Figure 7b as a continuous 3D surface plot in top, front and iso views.

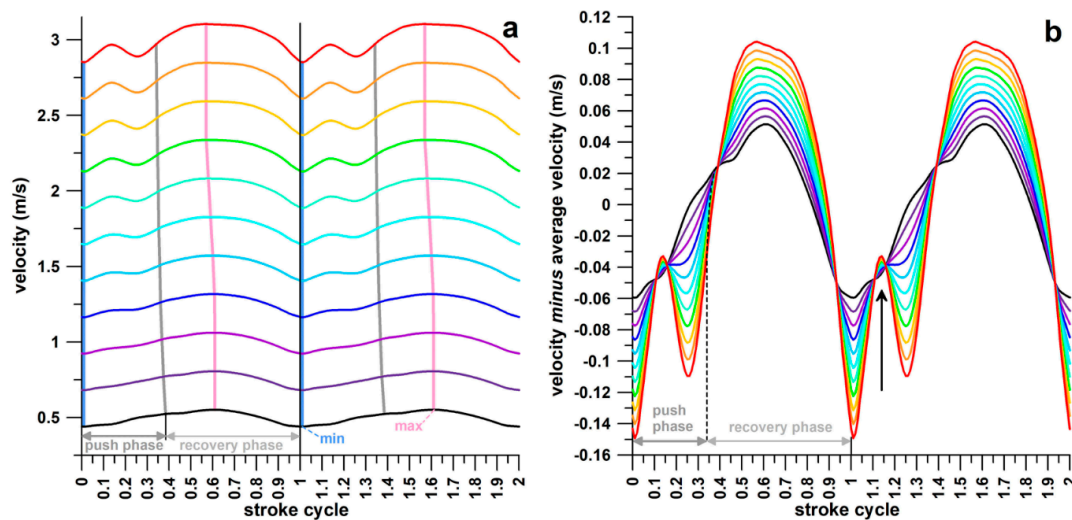


Figure 7. (a) Velocity profiles at different average velocities (0.5–3 m/s at 0.25 m/s steps) against the stroke cycle; min and max: lines where minimum and maximum velocities are located relative to the stroke cycle. (b) Fluctuations in the velocity around the average velocity against the stroke cycle; the arrow indicates the position of the temporary peak found at 15% of the stroke cycle.

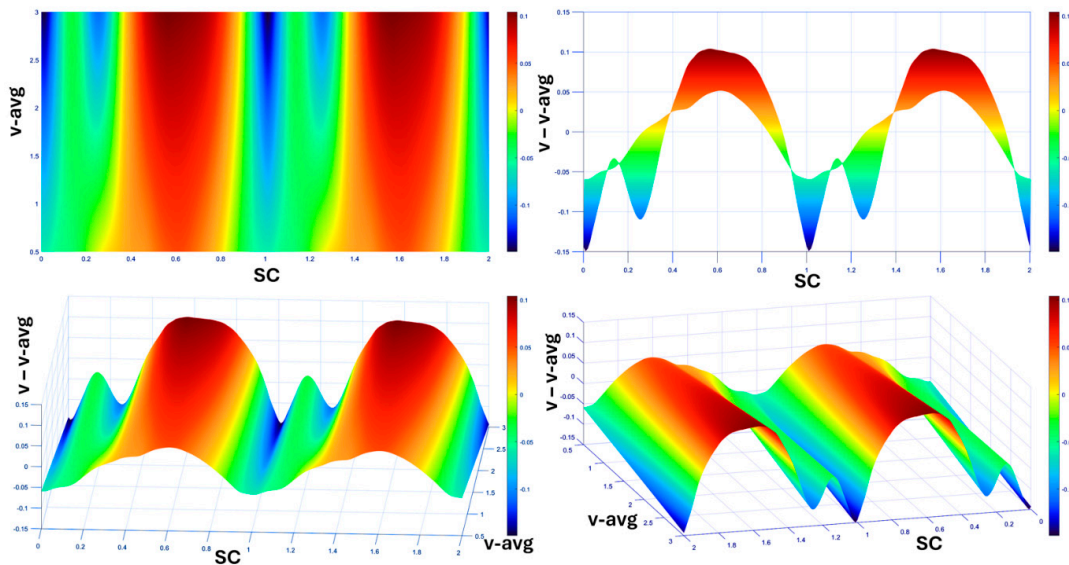


Figure 8. Continuous 3D surface plots in top (upper row left), front (upper row right) and iso views (bottom row); the velocity fluctuations ($v-v\text{-avg}$) in Figure 7b are plotted against the average velocity ($v\text{-avg}$) and the stroke cycle (SC) and the colour coding refers to the velocity fluctuations.

3.1.3. Experiment 1—Acceleration Profile

Figure 9 shows the acceleration data derived from the raw velocity data shown in Figure 3 as an example, averaged across a window with a width of 1.88% of the stroke cycle. Figure 10 shows the acceleration data derived from the velocity data shown in Figure 7a. Both Figures 9 and 10 show comparable results, characterised by three initial spikes, an upward spike, a downward spike and another upward peak; the magnitudes of these are highly velocity-dependent. The first part of the third peak is in the push phase; the second part in the recovery phase. Between 50% and 75% of the stroke cycle, the acceleration has no apparent velocity dependence, which gradually changes from positive to negative (unlike the sharp and sudden zero transitions associated with the first three spikes). The end of the recovery phase shows a clear downward spike. Figure 11 shows the data of Figure 10 as a continuous 3D surface plot in top, front and iso views. In Figure 11, the zero line is in the lime-green ribbon.

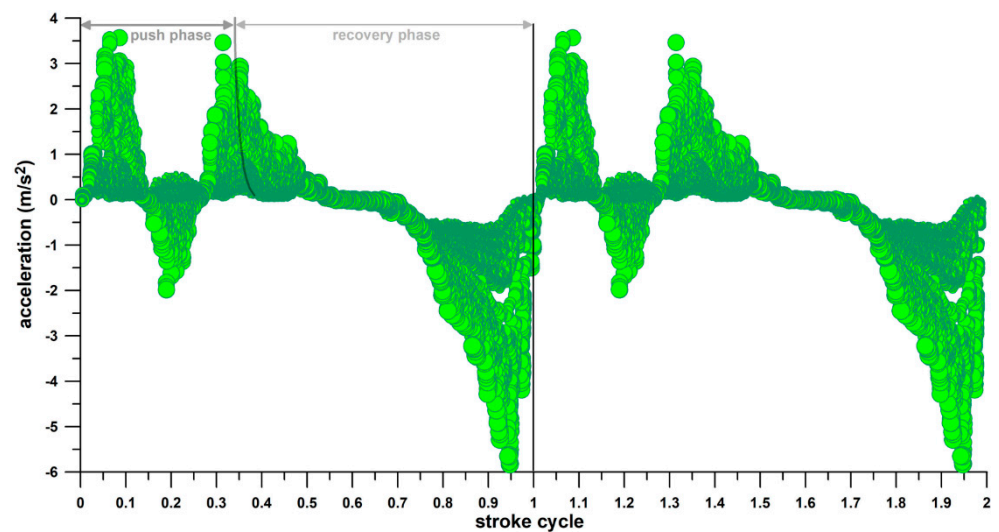


Figure 9. Bubble plot of the raw acceleration data (64 k data; averaged across a window with a width of 1.88% of the stroke cycle) against the stroke cycle; the bubble size refers to the average velocity of the stroke cycle.

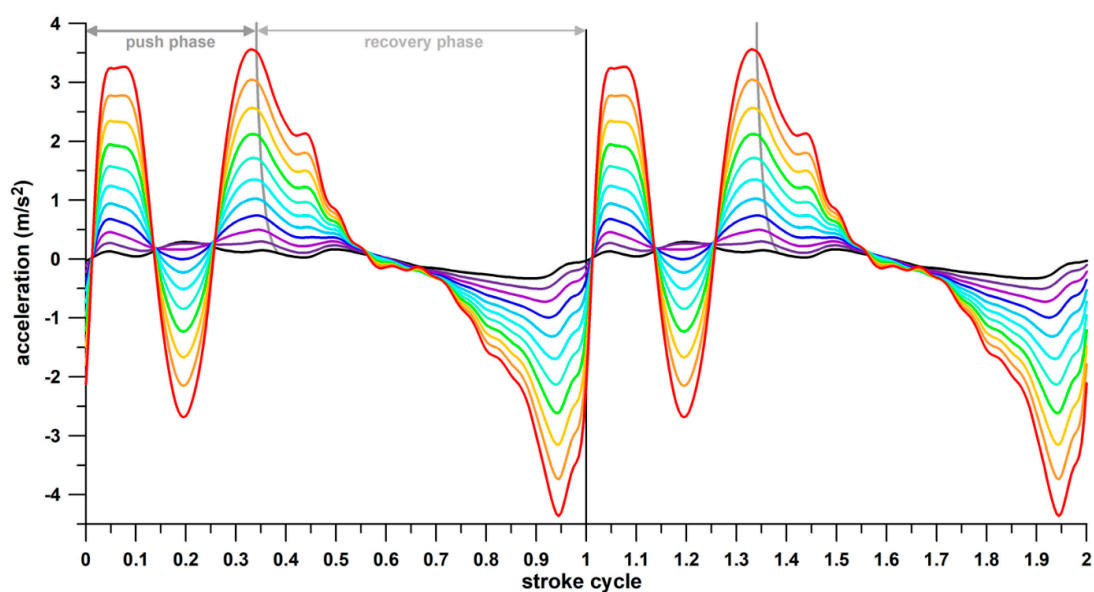


Figure 10. Acceleration profiles at different average velocities (0.5–3 m/s, at 0.25 m/s steps) against the stroke cycle; the colour coding is the same as in Figure 7.

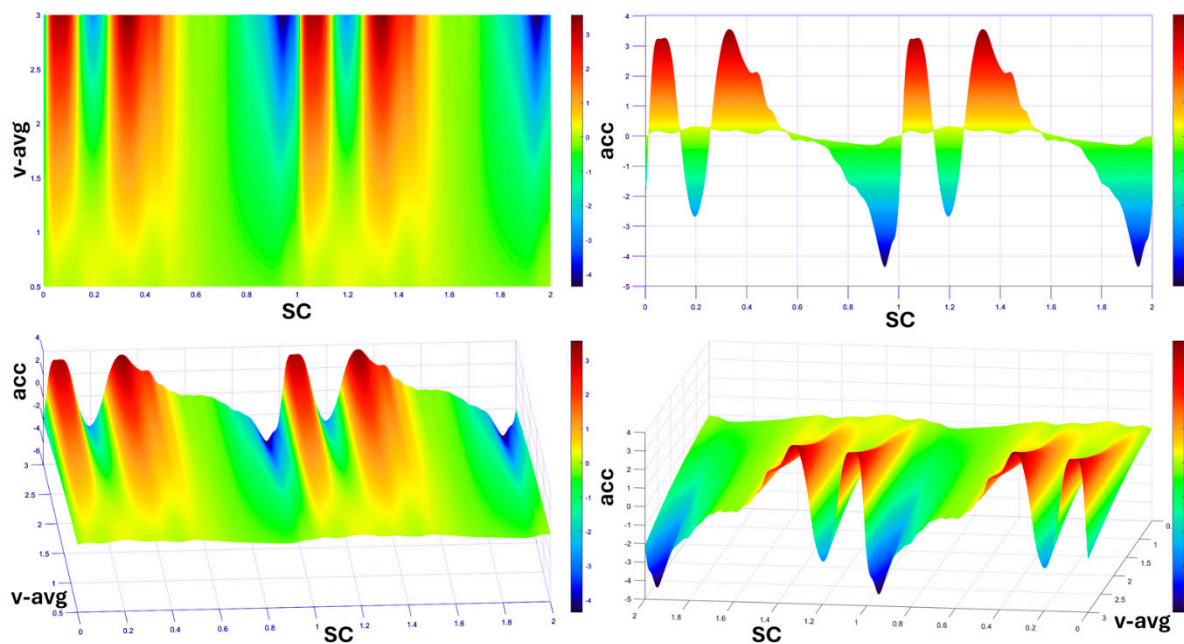


Figure 11. Continuous 3D surface plots in top (upper row left), front (upper row right) and iso views (bottom row); the acceleration (acc) of Figure 10 is plotted against the average velocity (v-avg) and the stroke cycle (SC) and the colour coding refers to the magnitude of the acceleration.

What all speed levels had in common was that the speed continued to increase after the end of the push phase (Figures 3 and 7). As the participant kept his trunk slightly bent forward in a static position throughout the experiments, the only translationally moving masses *within* the user–wheelchair system were the participant’s arms. In fact, the participant could not move his trunk back and forth very well during the stroke cycle, as the duration of the stroke cycle was only 0.4 s at the maximum possible speed. The constantly accelerating and decelerating arms produced inertial forces that influenced the speed of the wheelchair frame, in addition to the propulsive forces generated by the participant and the dissipative forces such as rolling friction and aerodynamic drag. These three different influencing factors cannot be directly broken down into their individual contributions. To this end, further experiments with the same participant were conducted, but with the wheelchair statically mounted on a force plate (Kistler, Winterthur, Switzerland).

3.2. Experiment 2

In the first test (Figure 12a), the wheels were unconstrained. Therefore, the speed hardly decreased during the recovery phase. Furthermore, due to the relatively high speed (3.3 m/s, 13 kph), the participant was not able to move his hands at the same speed when gripping the pushrim at the beginning of the push phase. Therefore, the speed dropped sharply, followed by a steep increase and a slight decrease immediately before the end of the push phase. The forces recorded by the force plate were the reaction forces that balance the inertial forces generated by the moving arms in the forward–backward and up–down directions (Figure 12a). The horizontal force F_y is negative in the second half of the recovery phase and in the push phase, which corresponds to a backward deceleration (dec_B ; Figure 12a) of the arm in the second half of the recovery phase and to a forward acceleration (acc_F ; Figure 12a) in the push phase. The horizontal force F_y is positive in the first half of the recovery phase, corresponding to a forward deceleration (dec_F ; Figure 12a) of the arm followed by a backward acceleration (acc_B ; Figure 12a). The vertical force F_z shows a comparable action in Figure 12a, namely positive in the push phase (downward acceleration), negative in the first part of the recovery phase (downward deceleration + upward acceleration), and predominantly positive in the remaining part of the recovery phase (upward acceleration).

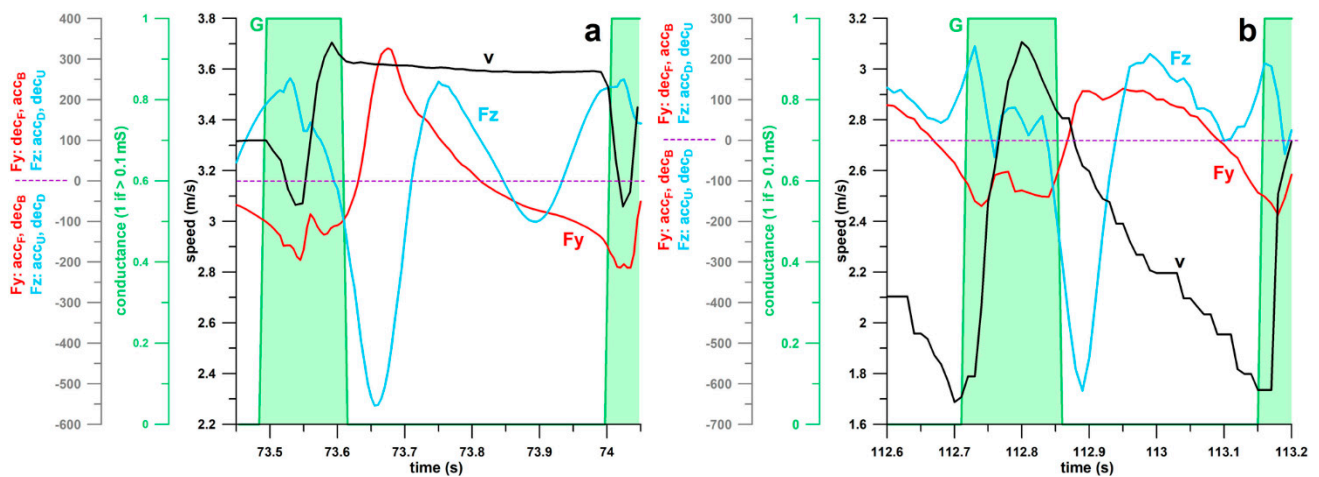


Figure 12. Wheel speed (v , converted to m/s), normalised conductance (G , 1 if >0.1 mS), and the horizontal (F_y) and vertical (F_z) inertial forces of the arms against the time, while the wheelchair was mounted statically on a force plate: (a) unconstrained freely spinning wheels; (b) wheel movement constrained by an ergometer. The dashed purple line indicates the zero-force level; F_z is shown as a net force as the system weight was set to zero during calibration of the force plate; the green shaded area corresponds to the push phase; acc_F = acceleration forward; acc_B = acceleration backward; dec_F = deceleration forward; dec_B = deceleration backward; acc_U = acceleration upward; acc_D = acceleration downward; dec_U = deceleration upward; dec_D = deceleration downward.

In the second test, the wheels were constrained by an ergometer (Cycling Deal, Dandenong South, Australia), equally mounted on the force plate with the wheelchair placed on top of it. This experimental setup resulted in a rapid velocity drop of approximately 1.3 m/s, from 3.1 to 1.8 m/s within 0.3 s (Figure 12b). In addition, the speed began to decrease already at the end of the push phase. The forces of F_y and F_z showed a comparable effect which can already be seen in Figure 12a. The peak forces ranged from 100 to 600 N at the velocities shown in Figure 12, with specific ranges as follows: positive F_y : 100–300 N; negative F_y : 100–200 N; positive F_z : 200–300 N; negative F_z : 500–600 N. The impulses of F_y and F_z in Figure 12a were -2.61 and -1.25 Ns, respectively. The impulses of F_y and F_z in Figure 12b were 1.14 and -0.33 Ns, respectively.

3.3. Wheelchair Model with Moving Masses

The input data required for calculating DF and RF were obtained from the coast-down experiments in the form of two constants:

- $c_1 = 0.5 \rho Ad + k m g = 1.121$, which leads to a drag area Ad of approximately 1.8 m^2 (neglecting the velocity-dependent rolling friction);
- $c_2 = \mu m g = 12.9 \text{ N}$, which results in a rolling friction coefficient μ of 0.0122.

Accordingly, RF was approximately 12.9 N, and DF was approximately 7 N at an average speed of 2.5 m/s. The propulsive force PF required to counteract the two dissipative forces, while maintaining an average constant velocity, was 62 N at the plateau level during the push phase (Figure 13a). Figure 13b shows the force profiles of five different F_y levels (100%, 75%, 50%, 25%, 0% F_y). Figure 13c shows the corresponding velocity profiles related to the five different F_y levels. Reducing F_y had no influence on the propulsive force PF , which remained constant at 62 N. This result is not surprising and is actually logical since the force profiles satisfied the conditions of Equations (4)–(7).

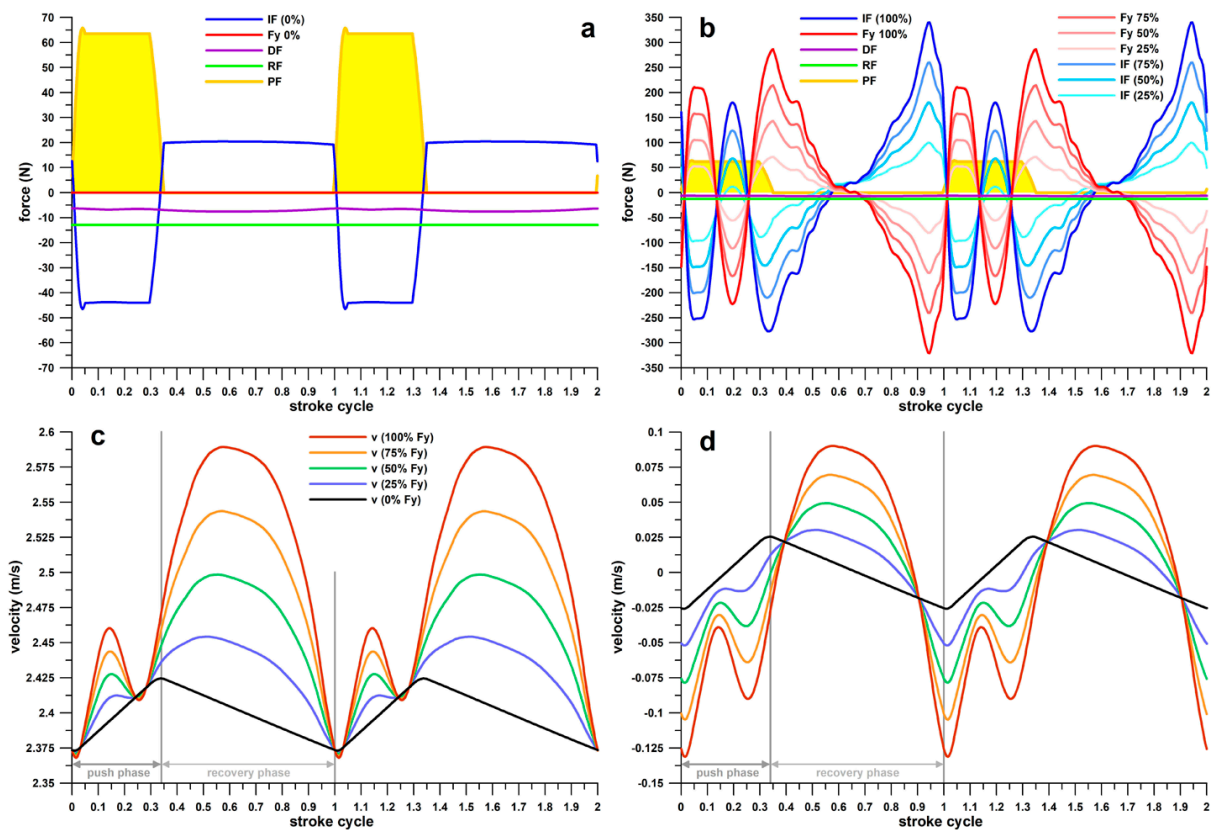


Figure 13. Forces (a,b) and velocities (c,d) against the stroke cycle, resulting from the model. IF = inertial force of the system; F_y = horizontal inertial force of the moving arms; DF = aerodynamic drag force; RF = rolling resistance force; PF = propulsive force; F_y 100%, F_y 75%, F_y 50%, F_y 25%, F_y 0% = F_y expected, i.e., at 100%, or magnitude of F_y reduced to 75%, 50%, 25% and 0%, respectively; IF (100%), IF (75%), IF (50%), IF (25%), IF (0%) = IF if F_y is at 100%, 75%, 50%, 25%, or 0%, respectively; v = velocity of the wheelchair frame; v (100% F_y) = velocity if F_y is at 100%; the yellow shaded area corresponds to the push phase. Note that (c) shows only the evolution of the velocity fluctuations when changing F_y ; therefore the 5 velocity profiles do not have exactly the same average velocity; (d) shows the velocity fluctuations about the average velocity (2.45 m/s for all 5 profiles).

The evolution of the velocity profiles (Figure 13c) as F_y increases from 0% to 100% explains the phenomenon that the velocity continues to increase after the end of the push phase, as seen in Figures 3 and 7. The velocity profile at 0% F_y (corresponding to massless arms) is approximately triangular. The velocity increases from the initial velocity to a maximum velocity at the end of the push phase (Figure 13c,d). This increase is due to the positive impulse of the sum of PF, DF, and RF (note that DF and RF are negative; Figure 13a). In the recovery phase, the velocity decreases from the maximum velocity to the initial velocity at the end of the recovery phase (Figure 13c). Increasing F_y leads to bulging of the near-straight velocity segments of the push and recovery phases (Figure 13c). In this model, the speed continues to increase after the end of the push phase if the increase in F_y is greater than 9%. Any further increase in F_y leads to more pronounced velocity fluctuations. The moving masses of the arms are solely responsible for this phenomenon. The velocity and acceleration profiles shown in Figures 7, 8, 10 and 11 are simply an effect of these moving masses.

When including the vertical force F_z in the wheelchair model, ranging between +223 N and −516 N, then the force RF is no longer constant (12.9 N), since RF is the product of μ and the normal force (usually the gravitational force, but influenced by F_z in this case). Consequently, the velocity profile would be affected locally, specifically at the

times of maximum and minimum force. Comparing the velocity profiles at 100% F_y and 0% F_z with those at 100% F_y and 100% F_z , the maximum local difference between these velocity profiles is only 0.002 m/s (0.08% of the average velocity). This result indicates that F_z (via RF), unlike F_y (via IF), does not significantly influence the behaviour of the velocity.

4. Discussion

This study provides evidence that the increase in the wheelchair velocity after the end of the push phase is solely due to the moving arm masses. If the trunk also moved during propulsion, this principle would extend to the moving trunk mass too. The arms reciprocating during a stroke cycle can be compared to the slider of a crank-slider mechanism, e.g., the slider of a shaping machine moving at a constant crank speed. If the acceleration or inertial force of the crank is integrated over a stroke cycle, regardless of the crank position in which the cycle starts, then the integrals are always zero, i.e., $\Delta v = 0$ and $\Delta S = 0$, and thus $\Delta p = m \Delta v = 0$. If the integrals were not zero but smaller or greater than zero, then $S < 0$ would remove energy from the system, F_y would become a dissipative force, and the wheelchair would continuously slow down due to arm movements. Conversely, if $S > 0$, the reciprocating arms would supply energy to the system, an assumption that already failed in Leonardo da Vinci's perpetual mobile machines. Due to the law of conservation of momentum, reducing the magnitude of F_y has no effect on the propulsive force PF at all. Therefore, using an alternative propulsion style, namely alternating left and right strokes rather than symmetrical pushing, where the actions of the two arms are out of phase by 50% of the stroke cycle, provides no advantage, at least at a constant average speed. If the actions of the two arms are opposite, they do not cancel each other out. The force F_y will definitely decrease but also be twice as frequent. However, the magnitude of PF remains unchanged.

As already mentioned in Section 1, de Vries et al. [13] assumed that the only forces acting on a wheelchair in everyday use are the propulsive and the resistive forces (which would produce a triangular velocity profile shown in Figure 13c). Based on this assumption, it seems correct to identify the beginning or end of the push phase based on the minimum or maximum velocity data, respectively. De Vries et al. [13] benchmarked this method against the SMARTWheel data and realised that “. . . the push durations derived from the IMU data were longer than those from the Smartwheel data . . .” [13]. The reason for this is that the velocity peak occurs well after the end of the push phase (Figure 7).

To understand the behaviour of the acceleration shown in Figure 10, one must remember that the propulsion of the wheelchair generated by the user can only be achieved through positive acceleration during the entire pushing phase. However, the acceleration during the push phase shown in Figure 10 is characterised by two positive spikes separated by a negative spike. During the recovery phase, the user-wheelchair system experiences a negative acceleration (deceleration), resulting from aerodynamic drag and rolling resistance. The former is a function of speed and frontal area (body position); the latter is a function of surface properties and the normal force. However, the acceleration during the recovery phase shown in Figure 10 is not entirely negative, but rather positive in the first part of the recovery phase (continuing the second positive spike of the push phase), approximately zero in the middle phase, and negative in the final phase. While most of the acceleration behaviour can be explained by the moving arm masses, the deceleration in the middle of the push phase is not immediately understandable. Since the magnitude of this deceleration is speed-dependent, it was assumed that the interaction of the user's hands and the pushrim is the cause of this deceleration. If this assumption is correct, the question must be asked why this deceleration in the experimental results of the static wheelchair tests (Figure 12) cannot be detected. In Figure 12a, the speed of the unconstrained wheel is so high that the user's hands cannot keep up with this speed at the beginning of the push phase. Therefore, the speed decreases immediately upon first contact with the pushrim and only accelerates in the second part of the push phase. However, in Figure 12b, the speed of the wheel, limited by the rollers of the ergometer, is so low (approximately 1.7 m/s translational

surface speed of the tyre) that the user's hands can accelerate the wheel upon first contact up to a speed of 3.1 m/s. The propulsion mechanisms of a rolling and a static wheelchair are evidently inherently different. Even the conditions of constrained and unconstrained wheels make a difference. Given these results, we agree with the assumptions of Basteris et al. [15], who found that the fluctuating speed during the push phase and particularly the decelerations are associated with inefficient coupling of the hand and pushrim. The temporary upward spike seen in the velocity profile in Figure 7 (arrow in Figure 7b) was also reported by Poulet et al. [3].

As shown in Section 3, the propulsive force depends only on the dissipative forces, and not on the forces caused by the movement of the arms (F_y). In this context, it is important to determine which of the two resistive forces has a greater influence on the propulsive force. In wheelchair racing, the coefficients of the resistive forces reported by Fuss [17] were $c_1 = 0.5 \rho A d + k m g = 0.08\text{--}0.09$; $c_2 = \mu m g = 6\text{--}8.3$ ($\mu = 0.01\text{--}0.012$). Chua et al. [18] reported average rolling friction coefficients μ of 0.0143 on a carpet floor, 0.0061 on a linoleum floor, and 0.0042 on a wooden floor. The results of the coast-down experiments shown in Section 3 were $c_1 = 1.121$ and $c_2 = 12.9$ ($\mu = 0.0122$). Although the rolling friction coefficients were comparable (likely due to similar floor materials, outdoor rubber track and indoor rubber floor), the aerodynamic coefficients ($0.5 \rho A d$) were fundamentally different due to the aerodynamic position that the wheelchair athletes assumed during the races. In court-based wheelchair sports (basketball, rugby, tennis), neither the wheelchair, apparel, nor posture follow any aerodynamic rules, simply because aerodynamics are not the primary factor affecting athlete performance. However, the aerodynamic resistance is speed-dependent: DF results from the product of c_1 and v^2 . Nowadays the speed v in wheelchair sports is conveniently measured with IMUs (gyro component); previously, it was measured using optical encoders [20] and electric DC motors/generators [17]. Van Dijk et al. [19] claimed that "Air resistance can be neglected during indoor wheelchair field and court sports". They support their claim with the argument that "As these [court] sports consist of short sprints and lots of braking, the wheelchair velocities are generally below 2.5 m/s" (9 kph). This argument is undoubtedly correct but does not support this assumption. For example, athletes with maximum speeds of 16–20 kph can produce a speed of more than 9 kph for 10–20% of the playing time [21]. In the model, the results of which are shown in Figure 13, the air resistance DF is 35% of the total resistance (sum of the dissipative forces) at an average stroke velocity of 2.5 m/s (9 kph). Neglecting DF (i.e., $DF = 0$ in the model), PF would drop by 36.1%. At a velocity of 1.25 m/s (4.5 kph; median speed of one athlete [21]), DF is 11.6% of the total resistance, and when neglecting DF , PF drops by 11.8%. At a velocity of 3.75 m/s (13.5 kph), DF is 55.8% of the total resistance, and when DF is neglected, PF decreases by 55.9%. These results clearly show that the air resistance cannot be assumed as negligible for indoor wheelchair court sports.

The limitations of this study are twofold:

First, the inertial force F_y of the mass of the moving arms could not be measured during experiment 1. For this reason, the wheelchair was mounted statically on a force plate to obtain a direct measurement. Although the movement patterns of the arms are generally comparable in rolling and static conditions, they are not exactly identical due to different constraint conditions of the wheels (rolling versus spinning-constrained and unconstrained). Therefore, F_y had to be calculated from the force equilibrium of a rolling wheelchair. However, F_y is certainly valuable for understanding the dynamics of the moving masses, but it has no effect on the propulsive force (Figure 13a). Calculations of athlete power and energy expenditure should be based on the propulsive force only, as the power values obtained from velocity profiles (Figure 7a), acceleration profiles (Figure 10), and system mass significantly overestimate the power, as noted by van Dijk et al. [19]. Particularly, the wheelchair user's positive power should be calculated only from the pure propulsive force that is required in the push phase to overcome the dissipative forces and that enables the gain or loss in speed per stroke cycle, but not directly from the measured velocity.

Second, there was only one participant in this study, who, moreover, was able-bodied. Although the participant had extensive experience driving a manual wheelchair, disabled wheelchair users may have a different propulsion style. Slowik et al. [22] described four propulsion styles (hand patterns, full-cycle hand paths) in individuals with complete motor paraplegia (arc, single loop, double loop, and semicircular). The participant's hand path used in the experiments of this study was an arc path. Regardless of the different hand path patterns, the principle of arm movement is similar in all four patterns, particularly for forward and downward movements in the push phase, followed by a backward movement of the arm in the recovery phase. The objective of this study was to investigate the dynamics of basic arm movements and their influence on the kinematics of the wheelchair. The extension of this objective to disabled wheelchair users and their different propulsion styles should cover not only constant speed but also different speeds, rolling resistances and accelerations.

Author Contributions: F.K.F., A.M.T. and Y.W. contributed equally to this research in terms of conceptualisation, development, methodology, fundamental research, data collection and analysis, and writing of the manuscript (original draft preparation and review and editing). All authors have read and agreed to the published version of the manuscript.

Funding: This research received no external funding.

Institutional Review Board Statement: The research was conducted according to the guidelines of the Declaration of Helsinki and approved by the Swinburne University Human Ethics Committee (approval no. 2019/106).

Informed Consent Statement: Informed consent was obtained from all subjects involved in the study.

Data Availability Statement: The data presented in this study are available on request from the first author to any qualified researcher who has obtained Ethics Approval for secondary use of existing data through a Consent Waiver.

Conflicts of Interest: The authors declare no conflicts of interest.

References

1. Vanlandewijck, Y.C.; Spaepen, A.J.; Lysens, R.J. Wheelchair propulsion efficiency: Movement pattern adaptations to speed changes. *Med. Sci. Sports Exerc.* **1994**, *26*, 1373–1381. [[CrossRef](#)] [[PubMed](#)]
2. van Dijk, M.P.; van der Slikke, R.; Berger, M.; Hoozemans, M.; Veeger, H. Look Mummy, No Hands! The Effect of Trunk Motion on Forward Wheelchair Propulsion. *ISBS Proc. Arch.* **2021**, *39*, 368–371.
3. Poulet, Y.; Brassart, F.; Simonetti, E.; Pillet, H.; Faupin, A.; Sauret, C. Analyzing Intra-Cycle Velocity Profile and Trunk Inclination during Wheelchair Racing Propulsion. *Sensors* **2023**, *23*, 58. [[CrossRef](#)]
4. Kawabata, K.; Ibusuki, T.; Mitsui, T.; Kamijo, Y.; Tajima, F. Kinematic Analysis of the Head and Trunk Movements of Quadriplegic Wheelchair Athletes in the Initial Acceleration Phase of the 100-m Sprint: A Case Study. *Int. J. Sport Health Sci.* **2024**, *22*, 34–41. [[CrossRef](#)]
5. Moss, A.D.; Fowler, N.E.; Goosey-Tolfrey, V.L. The intra-push velocity profile of the over-ground racing wheelchair sprint start. *J. Biomech.* **2005**, *38*, 15–22. [[CrossRef](#)] [[PubMed](#)]
6. Masson, G.; Bégin, M.-A.; Lopez Poncelas, M.; Pelletier, S.-K.; Lessard, J.-L.; Laroche, J.; Berrigan, F.; Langelier, E.; Smeesters, C.; Rancourt, D. Contribution of limb momentum to power transfer in athletic wheelchair pushing. *J. Biomech.* **2016**, *49*, 2577–2583. [[CrossRef](#)]
7. Fuss, F.K. Speed measurements in wheelchair sports—Theory and application. *Sports Technol.* **2012**, *5*, 29–42. [[CrossRef](#)]
8. Wu, H.W.; Berglund, L.J.; Su, F.C.; Yu, B.; Westreich, A.; Kim, K.J.; An, K.N. An instrumented wheel for kinetic analysis of wheelchair propulsion. *J. Biomech. Eng.* **1998**, *120*, 533–535. [[CrossRef](#)] [[PubMed](#)]
9. Cooper, R.A. SMARTWheel: From concept to clinical practice. *Prosthet. Orthot. Int.* **2009**, *33*, 198–209. [[CrossRef](#)] [[PubMed](#)]
10. Guo, L.; Kwarcia, A.M.; Rodriguez, R.; Sarkar, N.; Richter, W.M. Validation of a biofeedback system for wheelchair propulsion training. *Rehabil. Res. Pract.* **2011**, *2011*, 590780. [[CrossRef](#)] [[PubMed](#)]
11. Limroongreungrat, W.; Wang, Y.T.; Chang, L.S.; Geil, M.D.; Johnson, J.T. An instrumented wheel system for measuring 3-D pushrim kinetics during racing wheelchair propulsion. *Res. Sports Med.* **2009**, *17*, 182–194. [[CrossRef](#)] [[PubMed](#)]
12. Miyazaki, Y.; Iida, K.; Nakashima, M.; Maruyama, T.; Yamanobe, K. Measurement of push-rim forces during racing wheelchair propulsion using a novel attachable force sensor system. *Proc. Inst. Mech. Eng. Part P J. Sports Eng. Technol.* **2020**, *237*, 109–118.

13. de Vries, W.H.K.; van der Slikke, R.M.A.; van Dijk, M.P.; Arnet, U. Real-Life Wheelchair Mobility Metrics from IMUs. *Sensors* **2023**, *23*, 7174. [[CrossRef](#)] [[PubMed](#)]
14. Lewis, A.R.; Phillips, E.J.; Robertson, W.S.P.; Grimshaw, P.N.; Portus, M. Intra-Stroke Profiling of Wheelchair Propulsion Using Inertial Measurement Units. *Proceedings* **2018**, *2*, 256. [[CrossRef](#)]
15. Basteris, A.; Vigo, G.; Lentino, C.; Sanguineti, V. Definition of a protocol for geometric and kinematic measurements to assess wheelchair propulsion. In Proceedings of the XIX IMEKO World Congress, Fundamental and Applied Metrology, Lisbon, Portugal, 6–11 September 2009; pp. 2158–2161.
16. Le Rond d’Alembert, J.-B. *Traité de Dynamique*; M.-A. David (David l’aîné): Paris, France, 1743.
17. Fuss, F.K. Influence of mass on the speed of wheelchair racing. *Sports Eng.* **2009**, *12*, 41–53. [[CrossRef](#)]
18. Chua, J.J.C.; Fuss, F.K.; Subic, A. Rolling friction of a rugby wheelchair. *Procedia Eng.* **2010**, *2*, 3071–3076. [[CrossRef](#)]
19. van Dijk, M.P.; Hoozemans, M.J.M.; Berger, M.A.M.; Veeger, D.H.E. From theory to practice: Monitoring mechanical power output during wheelchair field and court sports using inertia measurement units. *J. Biomech.* **2024**, *166*, 112052. [[CrossRef](#)]
20. Moss, A.D.; Fowler, N.E.; Tolfrey, V.L. A telemetry-based velocometer to measure wheelchair velocity. *J. Biomech.* **2003**, *36*, 253–257. [[CrossRef](#)] [[PubMed](#)]
21. Fuss, F.K. Performance Analysis of Wheelchair Basketball Athletes. Chair of Biomechanics, Faculty of Engineering Science, University of Bayreuth: Bayreuth, Germany, 2024; unpublished results.
22. Slowik, J.S.; Requejo, P.S.; Mulroy, S.J.; Neptune, R.R. The Influence of Wheelchair Propulsion Hand Pattern on Upper Extremity Muscle Power and Stress. *J. Biomech.* **2016**, *49*, 1554–1561. [[CrossRef](#)] [[PubMed](#)]

Disclaimer/Publisher’s Note: The statements, opinions and data contained in all publications are solely those of the individual author(s) and contributor(s) and not of MDPI and/or the editor(s). MDPI and/or the editor(s) disclaim responsibility for any injury to people or property resulting from any ideas, methods, instructions or products referred to in the content.